Proceedings of the 2017 IEEE
International Conference on Robotics and Biomimetics
December 5-8, 2017, Macau SAR, China

Cycle Stability and Consumption Energy Efficiency Evaluation of Walking Stabilized by Stepping Feedforward and Visual-lifting Feedback

Keli Shen, Xiang Li, Izawa Daiji, and Mamoru Minami
Graduate school of Natural Science and Technology,
Okayama University, 3-1-1 Tsushima-naka, Kita-ku,
Okayama 700-8530, Japan
Email: {pue85qr6, pzkm87r2, p1k85fm}@s.okayama-u.ac.jp and minami-m@cc.okayama-u.ac.jp

***Abstract*—Biped locomotion created by control method based on Zero-Moment Point (ZMP) has been realized. However, this motion looks different from humans' walking since ZMP-based walking does not include tiptoe state. And when ZMP is on the tip of supporting foot, ZMP-control cannot work, making the humanoid tend to fall down. Besides, ZMP control lowers the humanoid robots' waist and keeps the knee bended, making robots walk like monkeys. Therefore, keeping the dynamical walking stable is a challenging issue for realizing human-like natural walking including tiptoe state. Our group has constructed dynamical walking model of humanoid robot including impact, point-contacting, surface-contacting and slipping of foot. And we have derived the dynamical equation by the Extended NE method. Combined control of Visual Lifting Approach and stepping feedforward is effective to stabilize biped walking without using ZMP. Walking efficiency is also an important issue to be discussed.**

I. Introduction

In many biped-walking control methods, ZMP-based walking control is considered as the efficient method, which has been certified to be useful for making practical biped-walking stable, since humanoid robots can keep the balance of walking and standing by retaining the ZMP within the convex hull of supporting area [1], [2]. However, ZMP control makes the robots' waist lower and keeps the knee bended, which makes humanoid robots look like monkeys' walking. Besides, other methods except ZMP have been proposed to keep the biped-walking trajectories inside a basin of attraction [3]-[5] that means stable walking, including a way being referred to limit cycle to determine input torque [6].

These previous methods are discussed based on simplified biped models. These researchers have not discussed the effects of tiptoe or slipping motion existing in practical environment. Different from the above researches, one study [7] has pointed out the effect of foot having many walking gaits such as surface-contacting and point-contacting. And the different walking states have their unique equations of motion and even the dimensions of the equations are not constant.

Our research has started from the view point of [7] to describe the dynamics of gaits including impact, point-contacting, surface-contacting and slipping/stick of the foot as correctly as possible. The published paper [8] has confirmed the accuracy and authenticity of the derived dynamical model using the mechanical energy-conservation law. The model in [7] only has foot without torso or body, while our model includes the dynamics of whole-body humanoid with arms and head [9]. In [9], dynamics of 21 kinds of gaits were derived. Varieties of model have been prepared for presenting dynamical walking transitions, like slipping/stick motion, point-contacting, surface-contacting, kicking off, etc. And what the authors should be noticed is that the dimensions of equations of motion are changed by the varieties of the biped-walking introduced in [10] concerning one-legged hopping robot.

Further the tipping over motion has been called non-holonomic dynamics including a joint such as free joint with no inputting torque. On the other hand, the heel or the toe of lifting foot in the air contacts with the ground geometrically. The referred paper [11] discussed a method of representing contacting with environment. It discussed that constraint motion with friction can be expressed by algebraic equation and applied to human configuration [12].

Visual-lifting Approach (VLA) based on visual servoing has been proposed that can realize a walking with slippage including toe-off state. Real-time position and orientation (pose) tracking method that measures humanoid's head pose by observing a 3D object has been proposed as visual pose estimation [13]. In our previous study about walking stabilized by VLA, the incomplete model of humanoid was applied in which head, arms and torso were neglected in [14], [15]. Thus, there have been some drawbacks, i.e., the model was too simple to consider the effect of dynamical coupling of arm and upper body. However, the renewed model [16]-[20] has been improved concerning the above problems, and the discussions of slipping and usefulness of the model have been proved in [9].

In [18], we used the feedback control onto joint angles of two legs to add the input torques for stepping forward, which made the joint angles change to certain degrees. Then we found that this type of walking behavior was different from our humans'. In our believing, humans when walking don't swing their legs forward by feedback control like robots' walking controlled by trajectory tracking, but they

978-1-5386-3741-8/17/$31.00 © 2017 IEEE

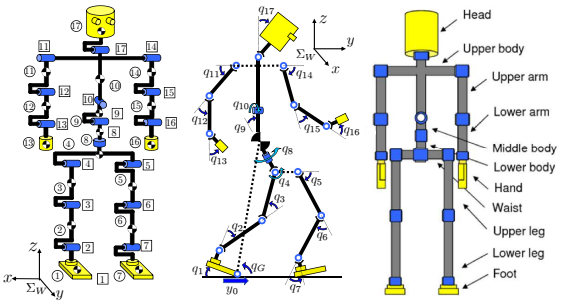

Fig. 1. Definition of biped-walking model, ①～⑰ represents link number, 1 ～ 17 is joint number, q_1～q_{17} is joint angles.

TABLE I
PHYSICAL PARAMETERS

Link	l_i[m]	m_i[kg]	d_i[Nms/rad]
Head	0.24	4.5	0.5
Upper body	0.41	21.5	10.0
Middle body	0.1	2.0	10.0
Lower body	0.1	2.0	10.0
Upper arm	0.31	2.3	0.03
Lower arm	0.24	1.4	1.0
Hand	0.18	0.4	2.0
Waist	0.27	2.0	10.0
Upper leg	0.38	7.3	10.0
Lower leg	0.40	3.4	10.0
Foot	0.07	1.3	10.0
Total weight [kg]	—	64.2	—
Total hight [m]	1.7	—	—

use feedforward oscillatory swinging. Therefore, in order to make humanoid robots walk like humans' walking, added feedforward inputs are used to keep the leg joints swinging for walking. Then, we verify that combination of visual-lifting feedback and swinging-out feedforwad has an ability to produce continuous walking motion in slippy environment by dynamical simulation. The simulation results indicate that swinging feedforward and visual lifting feedback are useful to stabilize biped-walking on the condition that humanoid's dynamics includes tiptoe, slipping and impact.

In this paper, we will introduce combined control method and analyze its walking efficiency on stabilizing walking by changing the visual-lifting gain and swinging-forward gain with dynamical evaluating measurements such as limit cycle [21], height of head and waist, step length, velocity, power and energy utilization.

II. DYNAMICAL MODEL BY NEWTON-EULER METHODOLOGY

A. Dynamical Model

The biped-walking robot in Fig.1 is discussed in this paper, Table I shows length l_i [m], mass m_i [kg] of links and coefficient of joints' viscous friction d_i [N·m·s/rad], which are determined by [22]. This model is simulated as a serial-link manipulator having branches and represents rigid whole-body such as feet including toe, torso, arms and so on and is up to 17 degree-of-freedom. Walking direction is along the y-axis. Though motion of legs is limited in sagittal plane, it generates many walking gaits since the robot has flat-sole feet and kicking torque. In this paper, the foot named as link-1 is defined as "supporting-foot" and the other foot named as link-7 is defined as "free foot" ("contacting-foot" when the floating foot contacts with ground) according to gaits. When the contacting-foot stops slipping which indicates that static friction force is exerted to the foot, the contacting-foot switches to supporting-foot and the previous supporting-foot is transfered into free foot if it was isolated from floor.

B. Forward Kinematic Calculations

In this paper, we derive the equation of motion following by NE formulation[14] [16]. So we must consider the structure of the supporting-leg with two situations. When the supporting-leg is constituted by rotating joint: We first have to calculate relations of positions, velocities and accelerations between links as forward kinetics procedures from bottom link to top link. Serial link's angular velocity ${}^i\boldsymbol{\omega}_i$, angular acceleration ${}^i\dot{\boldsymbol{\omega}}_i$, acceleration of the origin ${}^i\ddot{\boldsymbol{p}}_i$ and acceleration of the center of mass ${}^i\ddot{\boldsymbol{s}}_i$ based on Σ_i fixed at i-th link are obtained as follows.

$$ {}^i\boldsymbol{\omega}_i = {}^{i-1}\boldsymbol{R}_i^T\ {}^{i-1}\boldsymbol{\omega}_{i-1} + \boldsymbol{e}_{z_i}\dot{q}_i. \tag{1} $$

$$ {}^i\dot{\boldsymbol{\omega}}_i = {}^{i-1}\boldsymbol{R}_i^T\ {}^{i-1}\dot{\boldsymbol{\omega}}_{i-1} + \boldsymbol{e}_z\ddot{q}_i + {}^i\boldsymbol{\omega}_i \times (\boldsymbol{e}_{z_i}\dot{q}_i). \tag{2} $$

$$ \begin{aligned} {}^i\ddot{\boldsymbol{p}}_i = {}^{i-1}\boldsymbol{R}_i^T \Big\{ & {}^{i-1}\ddot{\boldsymbol{p}}_{i-1} + {}^{i-1}\dot{\boldsymbol{\omega}}_{i-1} \times {}^{i-1}\hat{\boldsymbol{p}}_i \\ & + {}^{i-1}\boldsymbol{\omega}_{i-1} \times ({}^{i-1}\boldsymbol{\omega}_{i-1} \times {}^{i-1}\hat{\boldsymbol{p}}_i) \Big\}. \end{aligned} \tag{3} $$

$$ {}^i\ddot{\boldsymbol{s}}_i = {}^i\ddot{\boldsymbol{p}}_i + {}^i\dot{\boldsymbol{\omega}}_i \times {}^i\hat{\boldsymbol{s}}_i + {}^i\boldsymbol{\omega}_i \times ({}^i\boldsymbol{\omega}_i \times {}^i\hat{\boldsymbol{s}}_i). \tag{4} $$

Then when the supporting-leg is constituted by prismatic joint. We will switch the equations as the following.

$$ {}^i\boldsymbol{\omega}_i = {}^{i-1}\boldsymbol{R}_i^{\mathrm{T}}\ {}^{i-1}\boldsymbol{\omega}_{i-1}. \tag{5} $$

$$ {}^i\dot{\boldsymbol{\omega}}_i = {}^{i-1}\boldsymbol{R}_i^{\mathrm{T}}\ {}^{i-1}\dot{\boldsymbol{\omega}}_{i-1}. \tag{6} $$

$$ \begin{aligned} {}^i\ddot{\boldsymbol{p}}_i = {}^{i-1}\boldsymbol{R}_i^{\mathrm{T}} \Big\{ & {}^{i-1}\ddot{\boldsymbol{p}}_{i-1} + {}^{i-1}\dot{\boldsymbol{\omega}}_{i-1} \times {}^{i-1}\hat{\boldsymbol{p}}_i \\ & + {}^{i-1}\boldsymbol{\omega}_{i-1} \times ({}^{i-1}\boldsymbol{\omega}_{i-1} \times {}^{i-1}\hat{\boldsymbol{p}}_i) \Big\} \\ & + 2({}^{i-1}\boldsymbol{R}_i^{T\,i-1}\boldsymbol{\omega}_{i-1}) \times (\boldsymbol{e}_z\dot{q}_i) + \boldsymbol{e}_z\ddot{q}_i. \end{aligned} \tag{7} $$

$$ {}^i\ddot{\boldsymbol{s}}_i = {}^i\ddot{\boldsymbol{p}}_i + {}^i\dot{\boldsymbol{\omega}}_i \times {}^i\hat{\boldsymbol{s}}_i + {}^i\boldsymbol{\omega}_i \times ({}^i\boldsymbol{\omega}_i \times {}^i\hat{\boldsymbol{s}}_i). \tag{8} $$

Here, ${}^{i-1}\boldsymbol{R}_i$ means orientation matrix, ${}^{i-1}\hat{\boldsymbol{p}}_i$ represents position vector from the origin of $(i-1)$-th link to the one of i-th, ${}^i\hat{\boldsymbol{s}}_i$ is defined as gravity center position of i-th link

and $\boldsymbol{e}_{z_i}$ is unit vector that shows rotational axis of i-th link. However, velocity and acceleration of 4-th link transmit to 8-th link and ones of 10-th link transmit to 11-th, 14-th and 17-th link directly because of ramification mechanisms.

C. Backward Inverse Dynamical Calculations

After the above forward kinetic calculation has been completed, contrarily inverse dynamical calculation from top to base link are shown as follows. Newton equation and Euler equation of i-th link are represented by Eqs. (9), (10) when ${}^i\boldsymbol{I}_i$ is defined as inertia tensor of i-th link.

$$
\begin{aligned}
{}^i\boldsymbol{f}_i &= {}^i\boldsymbol{R}_{i+1}{}^{i+1}\boldsymbol{f}_{i+1} + m_i{}^i\ddot{\boldsymbol{s}}_i && (9)\\
{}^i\boldsymbol{n}_i &= {}^i\boldsymbol{R}_{i+1}{}^{i+1}\boldsymbol{f}_{i+1} + {}^i\boldsymbol{I}_i{}^i\dot{\boldsymbol{\omega}}_i + {}^i\boldsymbol{\omega}_i \times ({}^i\boldsymbol{I}_i{}^i\boldsymbol{\omega}_i) \\
&\quad + {}^i\hat{\boldsymbol{s}}_i \times (m_i{}^i\ddot{\boldsymbol{s}}_i) + {}^i\hat{\boldsymbol{p}}_{i+1} \times ({}^i\boldsymbol{R}_{i+1}{}^{i+1}\boldsymbol{f}_{i+1}) && (10)
\end{aligned}
$$

On the other hand, since force and torque of 5-th and 8-th links are exerted on 4-th link, effects on 4-th link is shown as:

$$
\begin{aligned}
{}^4\boldsymbol{f}_4 &= {}^4\boldsymbol{R}_5{}^5\boldsymbol{f}_5 + {}^4\boldsymbol{R}_8{}^8\boldsymbol{f}_8 + m_4{}^4\ddot{\boldsymbol{s}}_4, && (11)\\
{}^4\boldsymbol{n}_4 &= {}^4\boldsymbol{R}_5{}^5\boldsymbol{n}_5 + {}^4\boldsymbol{R}_8{}^8\boldsymbol{n}_8 + {}^4\boldsymbol{I}_4{}^4\dot{\boldsymbol{\omega}}_4 + {}^4\boldsymbol{\omega}_4 \times ({}^4\boldsymbol{I}_4{}^4\boldsymbol{\omega}_4) \\
&\quad + {}^4\hat{\boldsymbol{s}}_4 \times (m_4{}^4\ddot{\boldsymbol{s}}_4) + {}^4\hat{\boldsymbol{p}}_5 \times ({}^4\boldsymbol{R}_5{}^5\boldsymbol{f}_5) \\
&\quad + {}^4\hat{\boldsymbol{p}}_8 \times ({}^4\boldsymbol{R}_8{}^8\boldsymbol{f}_8). && (12)
\end{aligned}
$$

Similarly, forces and torques of 11-th, 14-th and 17-th links transmit to 10-th link directly. Then, rotational motion equation of i-th link is obtained as Eq. (13) by making inner product of induced torque onto the i-th link's unit vector $\boldsymbol{e}_{z_i}$ around rotational axis:

$$\tau_i = \boldsymbol{e}_{z_i}^T\ {}^i\boldsymbol{n}_i + d_i\dot{q}_i. \quad (13)$$

However, when the supporting-foot (1-st link) is slipping (prismatic joint), the torque onto the 1-st link can be calculated by following equation.

$$\tau_1 = \boldsymbol{e}_{z_1}^T\ {}^1\boldsymbol{f}_1 + k_{f1}\dot{y}_1. \quad (14)$$

Finally, motion equation with one leg standing is written as:

$$\boldsymbol{M}(\boldsymbol{q})\ddot{\boldsymbol{q}} + \boldsymbol{h}(\boldsymbol{q},\dot{\boldsymbol{q}}) + \boldsymbol{g}(\boldsymbol{q}) + \boldsymbol{D}\dot{\boldsymbol{q}} = \boldsymbol{\tau}, \quad (15)$$

Here, $\boldsymbol{\tau}$ is input torque, $\boldsymbol{M}(\boldsymbol{q})$ is inertia matrix, both of $\boldsymbol{h}(\boldsymbol{q},\dot{\boldsymbol{q}})$ and $\boldsymbol{g}(\boldsymbol{q})$ are vectors which indicate Coriolis force, centrifugal force and gravity. When the supporting-leg is slipping, the $\boldsymbol{D} = diag[k_{f1}, d_1, d_2, \cdots, d_{17}]$ is a matrix which means coefficients of joints and between foot and ground. And $\boldsymbol{q} = [y_1, q_1, q_2, \cdots, q_{17}]^T$ means the angle of joints and the relative position between foot and ground.

III. Combined Biped-walking Control Method

1) Visual Lifting Approach for Keeping Standing and Walking: Visual Lifting Approach has been proposed, which can improve the stability of biped standing and walking as shown in Fig.2. We apply a model-based matching method to measure the posture of a static target object described by $\boldsymbol{\psi}(t) =$

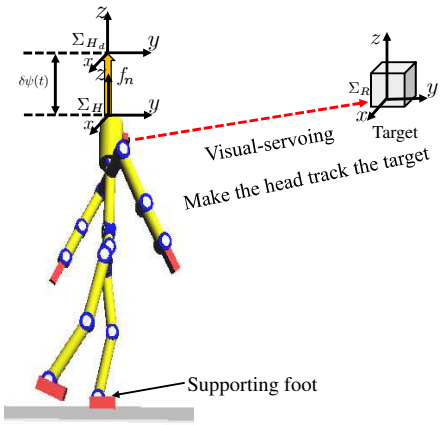

Fig. 2. Concept of Visual Lifting Stabilization.

$[X_{head}(t), Y_{head}(t), Z_{head}(t), \phi_{head}(t), \theta_{head}(t), \psi_{head}(t)]$ representing the position and orientation of robot's head based on Σ_H. The relatively desired head posture coordinate of Σ_R (coordinate of reference target object) and the current head posture coordinate Σ_H are predefined by Homogeneous Transformation as ${}^H\boldsymbol{T}_R$. The difference of the desired head posture coordinate Σ_{H_d} and the current head posture coordinate Σ_H is defined as ${}^H\boldsymbol{T}_{H_d}$, it can be described by:

$${}^H\boldsymbol{T}_{H_d}(\boldsymbol{\psi}_d(t), \boldsymbol{\psi}(t)) = {}^H\boldsymbol{T}_R(\boldsymbol{\psi}(t)) \cdot {}^{H_d}\boldsymbol{T}_R{}^{-1}(\boldsymbol{\psi}_d(t)), \quad (16)$$

where ${}^H\boldsymbol{T}_R$ is calculated by $\boldsymbol{\psi}(t)$. $\boldsymbol{\psi}(t)$ can be measured by on-line visual posture evaluation proposed by [13]. However, we assume that this parameter is given directly. Here, the force is considered to be directly proportional to $\delta\boldsymbol{\psi}(t)$, which is exerted on the head to minimize the deviation $\delta\boldsymbol{\psi}(t)(= \boldsymbol{\psi}_d(t) - \boldsymbol{\psi}(t))$ calculated from ${}^H\boldsymbol{T}_{H_d}$. The deviation of the robot's head posture is caused by gravity force and the influence of walking dynamics. The joint torque $\boldsymbol{\tau}_h(t)$ lifting the robot's head up and forward is donated:

$$\boldsymbol{\tau}_h(t) = \boldsymbol{J}_h(\boldsymbol{q})^T\boldsymbol{K}_p\delta\boldsymbol{\psi}(t), \quad (17)$$

where $\boldsymbol{J}_h(\boldsymbol{q}) = [\boldsymbol{J}_{hx}(\boldsymbol{q}), \boldsymbol{J}_{hy}(\boldsymbol{q}), \boldsymbol{J}_{hz}(\boldsymbol{q})]^T$ is Jacobian matrix of the head posture against joint angles $\boldsymbol{q}$ from supporting foot to head including $q_1, q_2, q_3, q_4, q_8, q_9, q_{10}, q_{17}$, and $\boldsymbol{K}_p = [20, 290, K_{pz}]$ is lifting proportional gain like impedance control where K_{pz} is visual-lifting gain along z-axis direction that can determine that humanoid robots walk like humans or monkeys. K_{pz} also has special ranges to stabilize the walking. We apply these inputs to stop falling down caused by the influence of gravity or dangerous slipping gaits happening unpredictably during walking progress. We stress that the input torque for non-holonomic joint such as joint-1, τ_{h_1} in $\boldsymbol{\tau}_h(t)$ in Eq.(17) is zero for its free joint. $\delta\boldsymbol{\psi}(t)$ can show the deviation of the humanoid's position and orientation, however, only position is discussed in this study.

2) Swinging Feedforward for Feet and Body's Motion: Besides $\boldsymbol{\tau}_h(t)$, in order to make the floating-foot and supporting-foot step forward, input torques $\boldsymbol{\tau}_t(t) = [0, \tau_{t2}, \tau_{t3}, 0, \tau_{t5}, \tau_{t6}, \tau_{t7}, 0, \cdots, 0]^T$ on two legs' joints are added. And another kind of input torques $\boldsymbol{\tau}_w(t) = [0, \cdots, 0, \tau_{w8}, 0, \cdots, 0]^T$ added on waist joint is used to swing the roll angle of the waist (joint-8) according to which foot is supporting foot, which further swings two arms with opposite directions by dynamical coupling. Here, $\boldsymbol{\tau}_t(t)$ and $\boldsymbol{\tau}_w(t)$ are seen as feedforward input torques. Here, t_2 means the time that supporting-foot and contacting-foot are switched. The elements $\boldsymbol{\tau}_t(t)$ and $\boldsymbol{\tau}_w(t)$ are shown below:

$$\tau_{t2} = DA_{t2} sin(w_{t2}(t - t_2)), \tag{18}$$

$$\tau_{t3} = D[-A_{t3} + A_{t3} sin(w_{t3}(t - t_2))]. \tag{19}$$

$$\tau_{t5} = \begin{cases} DA_{t51} cos(w_{t51}(t - t_2)), (t < 1.0[s]) \\ DA_{t52} cos(w_{t52}(t - t_2)), (t \geq 1.0[s]). \end{cases} \tag{20}$$

$$\tau_{t6} = D[-A_{t6} + A_{t6} sin(w_{t6}(t - t_2))]. \tag{21}$$

$$\tau_{t7} = \begin{cases} DA_{t71}, (\text{floating, } q_7 \leq 0.6[rad]) \\ -DA_{t72}, (\text{contacting, } q_7 \geq 0.35[rad]) \\ DA_{t73}, (\text{in other cases}). \end{cases} \tag{22}$$

$$\tau_{w8} = \begin{cases} DA_{w8} sin(w_{w8}(t - t_2)), (\text{right foot}) \\ -DA_{w8} sin(w_{w8}(t - t_2)), (\text{left foot}). \end{cases} \tag{23}$$

Here, amplitudes of torques are set as $A_{t2} = 10[Nm]$, $A_{t3} = 10[Nm]$, $A_{t51} = 20[Nm]$, $A_{t52} = 15[Nm]$, $A_{t6} = 20[Nm]$, $A_{t71} = 60[Nm]$, $A_{t72} = 40[Nm]$, $A_{t73} = 0[Nm]$, $A_{w8} = 50[Nm]$. Natural angular frequencies of torques are set as $w_{t2} = 2\pi[rad/s]$, $w_{t3} = 2\pi[rad/s]$, $w_{t51} = 2\pi/1.45[rad/s]$, $w_{t52} = 2\pi/1.85[rad/s]$, $w_{t6} = \pi[rad/s]$, $w_{w8} = 2\pi/1.85[rad/s]$.

A. Combined Controller for Lifting, Stepping and Swinging

Combining three kinds of torque inputs in Eqs. (17)∼(23), the controller for biped motion is derived,

$$\boldsymbol{\tau}(t) = \boldsymbol{\tau}_h(t) + \boldsymbol{\tau}_t(t) + \boldsymbol{\tau}_w(t). \tag{24}$$

IV. Calculation of Input Energy and Mechanical Energy

Input energy E_{input} of whole body while walking can be calculated by the following equation,

$$E_{input} = \sum_{i=1}^{17} \int_0^t \tau(t)_i \dot{q}_i dt. \tag{25}$$

It is necessary to calculate the height of the center of gravity of each link before the calculation of the potential energy. We use the homogeneous transformation matrix to calculate it as following equation.

$${}^W z_{Gi} = {}^W z_i + \frac{{}^W z_{i+1} - {}^W z_i}{2}. \tag{26}$$

Here, ${}^W z_{Gi}$ means the height of C.o.G of i-th link in world coordinate system ${}^W z_i$ is the height of the joint which seen from the world coordinate. So, we can calculate the potential energy as following equation.

$$E_p = \sum_{i=1}^{17} m_i^W z_i g. \tag{27}$$

Here, E_p is the potential energy of the model. m_i is the mass of each link. g is the gravitational acceleration. Then, we can calculate the rotational energy as following equation.

$$E_k = \sum_{i=1}^{17} \frac{1}{2} {}^W \boldsymbol{\omega}_i^{TW} \boldsymbol{I}_i {}^W \boldsymbol{\omega}_i. \tag{28}$$

Here, E_k is the rotational energy of the model. $\boldsymbol{I}_i$ is the moment of inertia of each link. Then, we can also calculate the translational energy as following equation.

$$E_v = \sum_{i=1}^{17} \frac{1}{2} m_i {}^W \dot{\boldsymbol{r}}_{gi}^{TW} \dot{\boldsymbol{r}}_{gi}. \tag{29}$$

Here, E_v is the translational energy of the model, $\dot{\boldsymbol{r}}_{gi}$ is the translational velocity of C.o.G of i-th link. Finally, the mechanical energy can be derived as following equation.

$$E_Q = E_p + E_k + E_v. \tag{30}$$

Then, energy utilization is calculated:

$$\eta = E_Q / E_{input}. \tag{31}$$

V. Stability Verification and Analyses of Biped-walking Based on Combined Control Method

In the environment that sampling time is set as $2.0 \times 10^{-4}[s]$ and coefficient of friction between the foot and the ground is set as $\mu_s = 1.0$ (static friction coefficient), $\mu_k = 0.7$ (viscous friction coefficient), the walking simulation is done. The desired position of head is set as $\boldsymbol{\psi_d} = [0, 0, 2.30[m]]$. Concerning simulation environment, we used "Borland C++ Builder Professional Ver. 5.0" to make simulation program and "OpenGL Ver. 1.5.0" to display humanoid's time-transient configurations.

In this simulation, we set $K_{pz} = 1100, D = 1.0$ first to verify the stability of walking.

Figure 3 and 4 represent the relation of angle q_8 and angular velocity $\dot{q}_8$ of waist joint during 100 steps. It is related to the stability of walking. Fig.3 shows the initial phrase and transient phase (from 1-st step to 11-th step). In both phases, the movement of the waist includes varieties and does not converge to one trajectory. After entering the stable phase shown in Fig.4, the movement of the waist enters a limit cycle with a very small width because of dynamic chaos effect producing during the walking process.

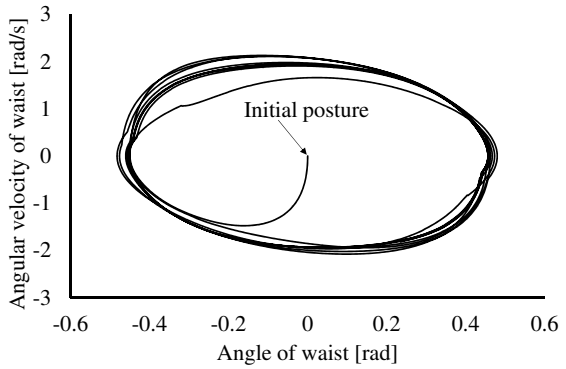

Fig. 3. Relation of angle q_8 and angular velocity $\dot{q}_8$ of waist joint in initial phase and transient phase (from the 1-st step to the 11-th step).

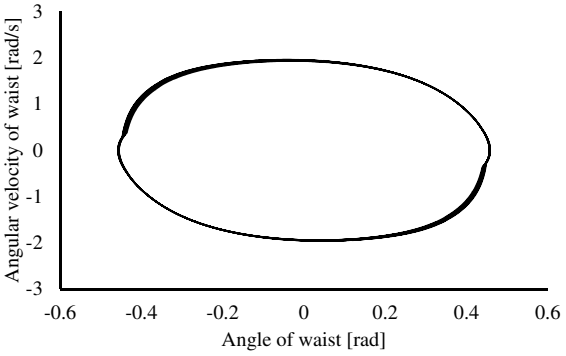

Fig. 4. Relation of angle q_8 and angular velocity $\dot{q}_8$ of waist joint in stable phase (after the 11-th step).

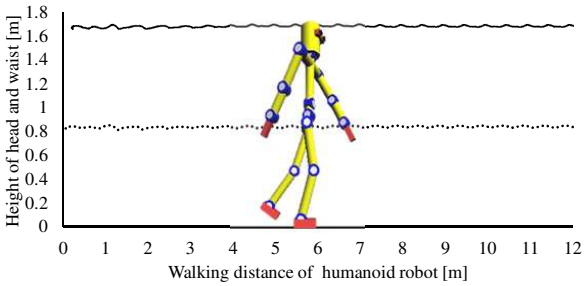

Fig. 5. Height trajectory of head and waist during walking process when $K_{pz} = 1100, D = 1.0$.

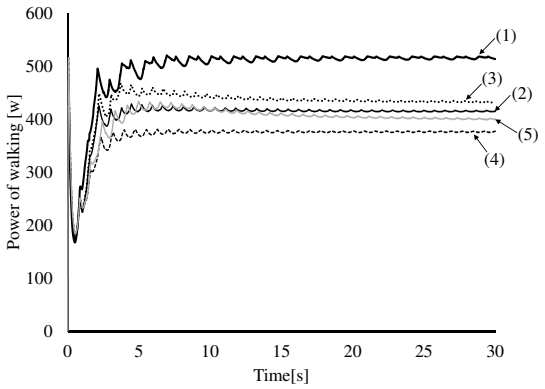

Fig. 6. Power of walking from case (1) to case (5) during $30[s]$ walking.

Figure 5 shows the height of head and waist during walking process when $K_{pz} = 1100, D = 1.0$. We can see that trajectories of height of head and waist change periodically after entering the stable phase.

Then, we did five cases of simulations to analyze the efficiency of walking by combined control under different circumstances by changing the visual-lifting gain $\boldsymbol{K}_p$ and swinging-feedforward gain D, which can be used to stabilize the walking:
(1) $\boldsymbol{K}_p = diag[20, 290, 1000]$, $D = 1.2$;
(2) $\boldsymbol{K}_p = diag[20, 290, 1050]$, $D = 1.0$;
(3) $\boldsymbol{K}_p = diag[20, 290, 1050]$, $D = 1.2$;
(4) $\boldsymbol{K}_p = diag[20, 290, 1100]$, $D = 0.8$;
(5) $\boldsymbol{K}_p = diag[20, 290, 1100]$, $D = 1.0$.

Our humanoid robot walks along the gait transition route-2 including stick and slip motion described in published paper [9]. The results of simulations are shown in Table II, where we can compare the dynamical parameters and evaluating measurements to analyze the stability of walking. Table II shows the step length of biped walking is influenced by the scale coefficient D existing in feedforward inputs while visual lifting gain is set as $\boldsymbol{K}_p = diag[20, 290, 1050]$. Step length in case (3) is bigger than in case (2), indicating that more feedforward inputs make humanoid robot walk in larger step length. Table II also shows that visual-lifting gain also has an effect on step length. Step length in case (5) is larger than one in case (2) and step length in (3) is larger than one in case (1). Similarly, more visual lifting torques can make the step length larger. Besides, we can see that the energy utilizations in all cases are low since viscous loss energy and collision loss energy are high during walking process.

Figure 6 shows the change of power of walking during $30[s]$ in five cases. From Fig.6, we can see that as the visual-lifting gain $\boldsymbol{K}_p$ increases, power of walking decreases: (1)→((3), (2))→((5), (4)). However, as D in feedforward input torques increases, power of walking also increases: (2)→(3); (4)→(5). Comparing effect of $\boldsymbol{K}_p$ and the effect of D on power, we find that $\boldsymbol{K}_p$ plays a leading role in changing the power of walking. As we know, the low power is better for humanoid robots to walk than high power. Therefore, among the cases (1), (2), (3), (4), (5), the power in case (4) is the lowest to stabilize the walking. Besides, Table II shows that energy utilization is obtained as maximum while average power is obtained as minimum in case (4), which indicates that walking efficiency of our humanoid robot in case (4) is the highest one in walking progress. From this view point, visual-lifting gain $\boldsymbol{K}_p$ and swinging-feedforward gain D in case (4) is the best set to keep walking.

TABLE II
RESULTS OF SIMULATION IN FIVE CASES DURING $30[s]$ WALKING.

Case	Number of steps[step]	Step length[m]	Velocity[m/s]	Average power[w]	Input energy[J]	Mechanical energy[J]	Energy utilization
(1)	38	0.48	0.625	514 (Maximum)	7695	599	0.0778 (Minimum)
(2)	40	0.48	0.653	415	6225	602	0.0967
(3)	40	0.50	0.658	433	6529	608	0.0931
(4)	39	0.48	0.628	377 (Minimum)	5628	602	0.1070 (Maximum)
(5)	38	0.50	0.639	399	6074	607	0.0999

VI. CONCLUSION

In this paper, we introduced our new humanoid model including impact, point-contacting, surface-contacting and slipping of foot and derived the dynamical equation by the Extended NE method. We explained new combined control method. Then, we verified the stability of walking and evaluated the energy consumption by power and energy utilization of walking. In the future work, we try to reduce the effect of dynamical chaos, short the transient time and improve the energy utilization by reducing viscous loss energy and collision loss energy.

REFERENCES

[1] M. Vukobratovic, A. Frank and D. Juricic, "On the Stability of Biped Locomotion," *IEEE Transactions on Biomedical Engineering*, Vol.17, No.1, 1970.

[2] M. Vukobratovic and J. Stepanenko, "On the Stability of Anthropomorphic Systems," *Mathematical Biosciences*, Vol.15, pp.1-37, 1972.

[3] S. Colins, A. Ruina, R. Tedrake and M. Wisse, "Efficient Bipedal Robots Based on Passive-Dynamic Walkers," *Science*, Vol.307, pp.1082-1085, 2005.

[4] J. Pratt, P. Dilworth and G. Pratt, "Virtual Model Control of a Bipedal Walking Robot," *Proceedings of IEEE International Conference on Robotics and Automation*, pp.193-198, 1997.

[5] R.E. Westervelt, W.J. Grizzle and E.D. Koditschek, "Hybrid Zero Dynamics of Planar Biped Walkers," *IEEE Transactions on Automatic Control*, Vol.48, No.1, pp.42-56, 2003.

[6] Y. Harada, J. Takahashi, D. Nenchev and D. Sato, "Limit Cycle Based Walk of a Powered 7DOF 3D Biped with Flat Feet," *Proceedings of IEEE/RSJ International Conference on Intelligent Robots and Systems*, pp.3623-3628, 2010.

[7] Y. Huang, B. Chen, Q. Wang, K. Wei and L. Wang, "Energetic efficiency and stability of dynamic bipedal walking gaits with different step lengths," *Proceedings of IEEE/RSJ International Conference on Intelligent Robots and Systems*, pp.4077-4082, 2010.

[8] X. Li, H. Imanishi, M. Minami, T. Matsuno, A. Yanou, "Modeling of humanoid dynamics including slipping with nonlinear floor friction," *Artif Life Robotics*, Vol.22 No.2, pp.175-183, 2017.

[9] X. Li, H. Imanishi, M.Minami, T. Matsuno and A. Yanou, "Dynamical Model of Walking Transition Considering Nonlinear Friction with Floor," *Journal of Advanced Computational Intelligence and Intelligent Informatics*, Vol.20 No.6, 2016.

[10] T. Wu, T. Yeh and B. Hsu, "Trajectory Planning of a One-Legged Robot Performing Stable Hop," *Proceedings of IEEE/RSJ International Conference on Intelligent Robots and Systems*, pp.4922-4927, 2010.

[11] Y. Nakamura and K. Yamane, "Dynamics of Kinematic Chains with Discontinuous Changes of Constraints—Application to Human Figures that Move in Contact with the Environments—," *Journal of RSJ*, Vol.18, No.3, pp.435-443, 2000.

[12] K.Yamane and Y.Nakamura, "Dynamics Filter - Concept and Implementation of On-Line Motion Generator for Human Figures," *IEEE Transactions on Robotics and Automation*, vol.19, No.3, pp.421-432, 2003.

[13] F. Yu, W. Song and M. Minami, "Visual Servoing with Quick Eye-Vergence to Enhance Trackability and Stability," *Proceedings of IEEE/RSJ International Conference on Intelligent Robots and Systems*, pp.6228-6233, 2010.

[14] W. Song, M. Minami, T. Maeba, Y. Zhang and A. Yanou, "Visual Lifting Stabilization of Dynamic Bipedal Walking," *Proceedings of 2011 IEEE-RAS International Conference on Humanoid Robots*, pp.345-351, 2011.

[15] W. Song, M. Minami and Y. Zhang, "A Visual Lifting Approach for Dynamic Bipedal Walking," *International Journal of Advanced Robotic Systems*, Vol.9, pp.1-8, 2012.

[16] A. Yanou, M. Minami, T. Maeba and Y. Kobayashi, "A First Step of Humanoid's Walking by Two Degree-of-freedom Generalized Predictive Control Combinedwith Visual Lifting Stabilization," *Proceedings of the 39th Annual Conference of the IEEE Industrial Electronics Society*, pp.6357-6362, 2013.

[17] Y. Kobayashi, M. Minami, A. Yanou and T. Maeba, "Dynamic Reconfiguration Manipulability Analyses of Humanoid Bipedal Walking," *IEEE International Conference on Robotics and Automation (ICRA)*,pp.4764-4769, 2013.

[18] X. Li,M. Minami, T. Matsuno, D. Izawa, "Visual Lifting Approach for Biped Walking with Slipping," *Journal of Robotics and Mechatronics*, Vol.29 No.3, pp.500-508, 2017.

[19] K. Shen, X. Li, H. Tian, D. Izawa and M. Minami, T. Matsuno, "Application and Analyses of Dynamic Reconfiguration Manipulability Shape Index into Humanoid Biped Walking," *IEEE International Conference on Robotics and Biomimetics*, pp1436-1441, 2016.

[20] T. Maeba, M. Minami, A. Yanou and J. Nishiguchi, "Dynamical Analyses of Humanoid's Walking by Visual Lifting Stabilization Based on Event-driven State Transition," *2012 IEEE/ASME Int. Conf. on Advanced Intelligent Mechatronics Proc*, pp.7-14, 2012.

[21] D. G. E. Hobbelen and M. Wisse, "Limit Cycle Walking," *Humanoid Robots: Human - like machines, Book edited by: Matthias Hackel, Itech, Vienna*, Austria, pp.277-294, 2007.

[22] M. Kouchi, M. Mochimaru, H. Iwasawa and S. Mitani, "Anthropometric database for Japanese Population 1997-98," *Japanese Industrial Standards Center (AIST, MITI)*, 2000.